ADVANCING LOW-COST MANGROVE ECOSYSTEM MAPPING: PRECISION VALIDATION OF IPHONE 12 PRO LIDAR FOR DTM GENERATION ACROSS CANOPY DENSITY GRADIENT

Sigit Bayhu IRYANTHONY [1], ***Anindya WIRASATRIYA*** [2*], ***Rudhi PRIBADI*** [3] ***& Pujiono Wahyu PURNOMO*** [4]

DOI: 10.21163/GT_2026.211.18

ABSTRACT

Precise Digital Terrain Models (DTMs) are essential for mangrove carbon accounting and Measurement, Reporting, and Verification (MRV) frameworks that facilitate climate change mitigation. Although airborne photogrammetry and LiDAR are frequently employed for terrain extraction, their utilization in dense mangrove wetlands is limited by elevated expenses and operational intricacies. This work offers a novel assessment of the iPhone 12 Pro LiDAR sensor as an economical and portable option for Digital Terrain Model (DTM) development in mangrove ecosystems, filling a significant void in accessible carbon monitoring technology. Utilizing the 3D Scanner App for iOS, the study gathered data from 12 locations (55 points per location) encompassing open regions, sparse canopies, and dense canopies, corroborated by 660 NRTK positioning points. The precision of the LiDAR-derived Digital Terrain Model (DTM) was assessed by extensive statistical criteria, such as Root Mean Square Error (RMSE), Mean Absolute Error (MAE), Bias, Pearson correlation coefficient, and 95% confidence intervals, thereby ensuring rigorous validation of consumer-grade mobile LiDAR for high-resolution topographic mapping. The results indicated exceptional accuracy in open environments (MAE < 0.1 m, negligible RMSE and bias), moderate precision in sparse canopies (MAE 0.086-0.381 m), and diminished performance in dense vegetation (MAE up to 1.064 m, positive bias of 0.928 m). Statistical analysis indicated negligible elevation fluctuation in open areas, however substantial outliers were seen in dense canopies. Regression analysis indicated a robust association in open areas (R^2 = 0.956), a moderate correlation in sparse vegetation (R^2 = 0.799), and a lesser correlation in dense canopies (R^2 = 0.663), implying possibility for enhancement by allometric modifications. Although professional LiDAR systems exhibit superior accuracy, the iPhone LiDAR is a pragmatic and cost-effective option for Digital Terrain Model production in open to moderately vegetated regions. The system's portability and affordability render it especially advantageous for ecological monitoring and geoscientific applications in resource-constrained environments, however dense vegetation poses significant challenges. These findings underscore the capability of consumer-grade LiDAR technology to facilitate precise environmental monitoring while markedly decreasing expenses relative to professional systems.

Keywords: *LiDAR; IPhone; DTM; Mangrove; Allometric.*

1. INTRODUCTION

Mangroves are salt-tolerant vegetation, comprising trees and shrubs, that flourish in coastal salty or brackish aquatic ecosystems (Shapiro, 2024). Mangrove has essential role for coastal region as the protector from great waves energy (Arnaud et al., 2023). Mangroves also offer the feeding and nursery

[1]*Doctoral Program of Aquatic Resources Management, Faculty of Fisheries and Marine Sciences, Universitas Diponegoro. Semarang, Indonesia; sigitbayhuiryanthony@gmail.com*
[2*]*Department of Oceanography, Faculty of Fisheries and Marine Science, Universitas Diponegoro, Semarang, Indonesia. Corresponding author: anindyawirasatriya@lecturer.undip.ac.id*
[3]*Department of Marine Science, Faculty of Fisheries and Marine Science, Universitas Diponegoro, Semarang, Indonesia; rudhipribadi@gmail.com*
[4]*Department of Aquatic Resource Management, Universitas Diponegoro, Semarang, Indonesia; purnomopoed@gmail.com*

ground for marine live cycle through its large and branched roots (Sasmito et al., 2023; Suwa et al., 2021). Its density coverage contributes to enhance carbon accumulation in coastal areas due to their advantageous intertidal location (Alongi, 2022; S. Song et al., 2023; Basyuni et al., 2023; Wirasatriya et al., 2022). Kauffman et al. (2018) discovered that mangroves possess a significantly greater carbon stock compared to terrestrial forests. This is attributed to their capacity to store more carbon both in their above-ground biomass and below the surface in their roots and sediment (e.g., Mcleod et al. 2011; Donato et al. 2011, 2012). The measurement of carbon biomass offers critical insights into facilitating biodiversity conservation and climate change mitigation initiatives (Amelia et al., 2023; Paul et al., 2023; Wainwright et al., 2023). Unfortunately, mangrove forests have historically experienced substantial reductions, decreasing from 225,000 km^2 in the 1970s to 137,000 km^2 by 2014, mostly owing to deforestation and deterioration (Friess et al., 2019; Lovelock et al., 2022). This loss has resulted in negative consequences (Arifanti et al., 2022), including weakened coastal protection, lower fisheries, heightened greenhouse gas emissions, and decreased ecosystem services such as nutrient cycling, which also impacts neighboring ecosystems like coral reefs and seagrass meadows (Bimrah et al., 2022; Friess et al., 2019).

The integration of satellite imagery with UAV-based photogrammetry is growing as an efficient technique for evaluating biomass in mangrove forests (Gao et al., 2022; Hu et al., 2020; Tian et al., 2023). Photogrammetry generates aerial photos, Digital Surface Models (DSM), and Digital Terrain Models (DTM) (Amuyou et al., 2022; Chan et al., 2021). Unfortunately, Digital Terrain Models generated by drones is limited in precision for wetland (tidal) regions. Basyuni et al., (2023) and Wirasatriya et al., (2022) utilize a Global Navigation Satellite Survey (GNSS) to develop a digital terrain model that facilitates the generation of canopy height models. Nevertheless, GNSS accuracy will decrease within the dense mangrove, resulting in a range of 0.6 to 10 meters. (Feng et al., 2021; Tomaštík & Everett, 2023). The other method options at the millimeter scale, void of canopy and signal constraints, may employ a water pass measurement or electronic total station; however, it necessitates more surveyors and a substantial expenditure (Jurado et al., 2020; Krause et al., 2019; Lynch et al., 2024). Thus, the DTM measurement causes the AGB investigation more costly and challenging for novice researchers with constrained financial resources.

Commencing in the 2020’s iPhone integrated the Light Detection and Ranging (LiDAR) sensor in both the iPhone and iPad Pro (Corradetti et al., 2022), utilized for measurement and 3D object scanning (Luetzenburg et al., 2021; B. Song et al., 2023; Teppati Losè et al., 2022). This concept has attracted significant attention in both consumer and professional domains, especially for uses in geosciences, historical documentation, and digital mapping (Kottner et al., 2023; Mêda et al., 2023). Initial assessments, like those by (Vogt et al., 2021a) and (Murtiyoso et al., 2021), have contrasted precision with the conventional techniques such as terrestrial laser scanning (TLS) and close-range photogrammetry. These studies illustrate that the iPhone 12 Pro LiDAR's is potential for particular applications, including industrial 3D scanning and heritage preservation (Teppati Losè et al., 2022), however it exhibits limitations in accuracy and elevated point cloud noise (Gollob et al., 2021a; Teo & Yang, 2023). Implementing LiDAR into mobile devices represents a significant advancement in the accessibility of advanced geospatial data collection for all individuals. This is particularly crucial in extreme situations (Teo & Yang, 2023), such as the identification of forests and wetland regions, where further research is evidently required (Gollob et al., 2021a).

The estimation of above-ground biomass (AGB) in mangrove ecosystems presents significant challenges, particularly in topographic mapping due to the dense canopy coverage (Basyuni et al., 2023; Wirasatriya et al., 2022). Traditional methods rely heavily on GNSS and interpolation data to construct Digital Terrain Models (DTMs) (Li et al., 2023; Raza et al., 2023), yet these techniques often suffer from high bias and poor signal reception due to canopy obstruction (Tong et al., 2023). In this context, the integration of the iPhone 12 Pro LiDAR offers a promising alternative for efficient, compact, and instant topographic scanning (Corradetti et al., 2022; Di Stefano et al., 2021). Capable of capturing point clouds at approximately 9,745 points per square meter, the iPhone 12 Pro LiDAR provides a convenient solution for dense canopy environments, though its point density is considerably lower than that of traditional terrestrial laser scanning (TLS) systems, which can achieve

around 469,856 points per square meter (Razali et al., 2022; Teppati Losè et al., 2022). Despite its potential, the application of iPhone 12 Pro LiDAR for AGB estimation, particularly in DTM development, remains underexplored. Nonetheless, with the growing adoption of LiDAR-equipped smartphones in multidisciplinary science, there is significant promise for advancing the accuracy and accessibility of mangrove ecosystem assessments.

Referring (Giri et al., 2011), Indonesia encompasses more than 3.39 million hectares of mangrove forests, representing roughly 22% of the global mangrove area. Estimating biomass in these environments is difficult (Basyuni et al., 2023; Wirasatriya et al., 2022), mostly due to GNSS field surveying limitations in marshes and forests, such as signal obstruction, multipath errors, and atmospheric influences (Tomaštík & Everett, 2023; Yang et al., 2020). This research seeks to address these issues by developing and validating novel allometric models that calibrate iPhone LiDAR-derived Digital Terrain Models (DTMs) for mangrove ecosystems and forests. This project aims to enhance the accuracy of allometric correction and the utilization of cost-effective LiDAR data for generating Digital Terrain Models (DTM) for biomass evaluation and various topographic applications. This is achieved by combining high-precision GNSS-RTK data with the characterization of mangrove canopy density. This will enhance environmental monitoring in complex coastal and forest ecosystems, making it more efficient and economical.

2. STUDY AREA

The study was conducted in Rembang Regency, focusing on the villages of Pasar Banggi, Tireman, and Kabongan Lor (6° 42'7.01"S - 111° 22'51.76"E, **Fig. 1**). This region encompasses approximately 36 to 45 hectares over a 3.8 km coastal line.

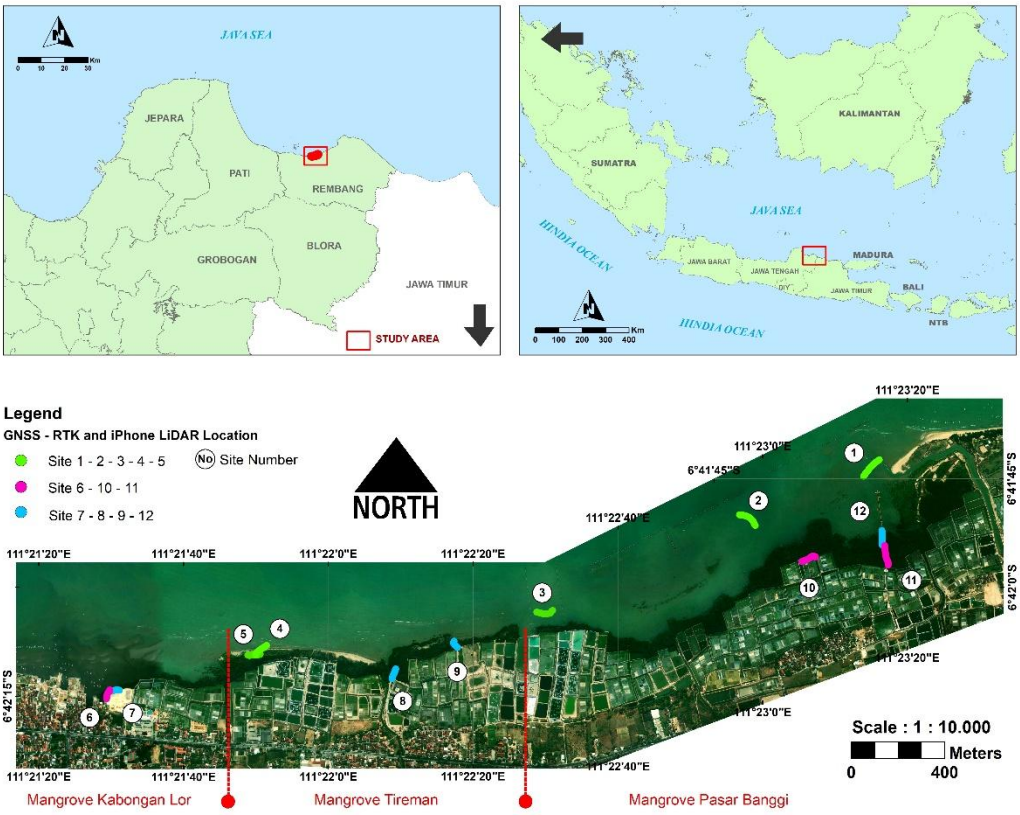

Fig. 1. Research location in Pasarbanggi, Tireman, and Kabonganlor, this site study 1-2-3-4-5 around the sand beach when the sea low tide, 6-10-11 in Dense mangrove canopy and 7-8-9-12 in Thin mangrove canopy.

This region is ever evolving and features a combination of sandy beaches, mudflats, rehabilitated mangrove forests, aquaculture ponds, and adjacent industrial facilities (Iryanthony, et al., 2025). The mangrove region comprises six primary tree species: Rhizophora apiculata, R. mucronata, R. stylosa, Avicennia marina, Excoecaria agallocha, Sonneratia. R. apiculata and R. mucronata are the predominant species, indicating the efficacy of the region's conservation initiatives (Iryanthony, et al., 2025; Iryanthony, et al., 2025; Soeprobowati et al., 2024).

The region comprises four distinct zones: the ocean, sandy shoreline, mangrove salt ponds, and populated areas, exemplifying a complex and diverse coastal environment (Bagas et al., 2024; Mustofa et al., 2023). The data collecting process occurred from October 11 to 14, 2024. The tidal dynamics in the coastal region of Rembang Regency indicated a rising tide began at 01:03 WIB, peaking at 04:22 WIB, followed by the ebb phase initiating at approximately 07:45 WIB and attaining the lowest tide point at 11:18 WIB. This tidal pattern is a component of the daily cycle shaped by the gravitational affects of the moon and sun, along with the local coastal topography. The northern section of the research site is a sandy beach plain, whereas the southern area consists of a mudflat that transitions into a mangrove forest. Beyond the mangroves are salt ponds and intense shrimp farms. Measurements in the open area were performed on the seashore plain, a highly exposed site devoid of vegetation and human settlements. The research site and the arrangement of sample sites are illustrated in **Fig 1**.

3. DATA AND METHODS

This section outlines a cohesive methodological framework aimed at maintaining consistency across data gathering, processing, and validation phases. The workflow is organized in a sequential manner, beginning with mobile LiDAR surface data collection, proceeding to high-precision GNSS measurements, and culminating in database integration and statistical validation. In this context, the iPhone 12 Pro LiDAR functions as the primary source of high-resolution elevation data, supplying the essential dataset for further studies. All resulting datasets were carefully aligned via georeferencing, ground control integration, and GIS-based processing to facilitate rigorous cross-comparison, uncertainty evaluation, and quantitative accuracy assessment.

3.1. iPhone 12 Pro LiDAR

The iPhone 12 Pro and iPhone 12 Pro Max feature a LiDAR (Light Detection and Ranging) sensor that improves depth-sensing functionality. The iPhone 12 Pro features a 12 MP camera system including three distinct cameras (1x telephoto, 1x wide, and 1x ultrawide), a flashlight, and a LiDAR sensor on the rear of the device (Kottner et al., 2023). The iPhone 12 Pro's rear camera assembly contains an iLiDAR module featuring a vertical cavity surface-emitting laser (VCSEL) as the emitter and a single-photon avalanche diode (SPAD) sensor integrated with a complementary metal-oxide semiconductor (CMOS) for signal detection (Gollob et al., 2021b; Mikalai et al., 2022; Vogt et al., 2021b). The VCSEL operates in the near-infrared (NIR) spectrum, at approximately 800 nm, generating a measuring array comprising 576 points, 12 x 12 dot matrix (Kottner et al., 2023) or 24 $\times$ 24 points per photon burst (King et al., 2023; Luetzenburg et al., 2021). The point density of this array adheres to a linear trajectory on a logarithmic scale, indicating that uncertainty increases with distance (7225 points per m^2 at 0.25 m, decreasing to 150 points per m^2 at 2.5 m) (Luetzenburg et al., 2021). In adequately illuminated environments, the iLiDAR module can measure distances up to 5 meters, possesses an instantaneous field of view (IFOV) of 90 degrees, and exhibits an average deviation of approximately 10 millimeters from the actual depth measurement (King et al., 2022, 2023).

The current investigation utilized LiDAR scanning with the 3D Scanner App (version 2.1.3) on iOS 18.2.1, obtained from the iOS App Store, consistent with a prior study (King et al., 2023b; Luetzenburg et al., 2021). Data acquisition was conducted at a scanning height of approximately 1–1.2 meters to guarantee uniform coverage throughout the surveyed region. The LiDAR point cloud

acquisition was set up with automated texturing, processing of small models, automatic orientation for diminutive items, and GPS-tagged scans to improve spatial referencing. GPS tagging was essential for enabling georeferencing corrections, given that the positional accuracy of field-acquired data fluctuated between 3 and 5 meters, as demonstrated by the 3D Scanner output in LAS format. The acquired high-density point cloud data were subsequently transferred into CloudCompare, an open-source LiDAR processing application (Kottner et al., 2023). In CloudCompare, Ground Control Points (GCPs) were implemented to enhance spatial precision, and the LAS point cloud was transformed into a 3D mesh representation (Luetzenburg et al., 2021). The processed data were ultimately exported in GeoTIFF format for subsequent spatial analysis and incorporation into Geographic Information System (GIS) procedures. This methodological approach guarantees superior terrain reconstruction, enhancing the capabilities of mobile LiDAR technology for accurate topographic mapping and geospatial analysis.

3.2. Real Time Kinematic (RTK) survey

The present investigation achieved precise coordinate collection using the Global Navigation Satellite System (GNSS) Geomate SG7 receiver. To enhance positional accuracy, the study utilized Network Real-Time Kinematic (NRTK) corrections (Nik Azhan Hakim et al., 2023; Zeybek et al., 2023; Zvirgzds & Celms, 2020), implementing a Continuously Operating Reference Station (CORS) within a 2‑6 km Line of Sight (LOS) for optimal performance (Ji et al., 2022; Yurdakul & Kalaycı, 2022). To ensure optimal performance, a stable internet or mobile network connection was maintained throughout the survey. The GNSS data (**Fig. 2)** was acquired while stationary, employing the Geomate SG7 NRTK method, which yielded highly precise measurements with a horizontal precision of 8 mm (Kanellopoulos et al., 2019; Pepe, 2018) and a vertical accuracy ranging from 15 mm to 25 mm for distances under 10 km (Bernstein & Janssen, 2022; Yurdakul & Kalaycı, 2022).

The NRTK approach facilitated swift location determination, attaining a fixed answer in roughly 5 seconds in unobstructed environments. Data collecting beneath dense mangrove canopies necessitated prolonged processing durations owing to signal attenuation. The research was carried out in three different environmental settings: sandy open fields, moderately dense canopy, and totally dense mangrove canopy. Each surveyed site consisted of 55 measurement points, with three identified as Ground Control Points (GCPs) at strategically chosen locations (samples 1, 23, and 55). This stringent process guaranteed precise geospatial data acquisition, facilitating dependable integration with LiDAR-derived datasets for high-resolution topographic assessment (**Table 1**).

Table 1.

The report provides a summary of the RTK survey's (mean) elevation in orthometric terms, sample size, standard deviation, standard error, and canopy cover classifications, as well as their typical locations and preparation guidelines for the survey.

Site condition	NDVI Class	Canopy	Site	N	Mean (m)	SD (m)
Coastal Sand Beach	-1 to 0,32	No	1	55	0,912	0,049
Coastal Sand Beach	-1 to 0,32	No	2	55	-0,224	0,053
Coastal Sand Beach	-1 to 0,32	No	3	55	-0,168	0,020
Coastal Sand Beach	-1 to 0,32	No	4	55	0,222	0,106
Coastal Sand Beach	-1 to 0,32	No	5	55	0,636	0,144
Thin mangrove canopy	0,43 to 1	High	6	55	1,002	0,398
Dense mangrove canopy	0,33 to 042	Mid	7	55	1,556	0,201
Dense mangrove canopy	0,43 to 1	High	8	55	0,327	0,121
Dense mangrove canopy	0,33 to 042	Mid	9	55	0,285	0,282
Thin mangrove canopy	0,33 to 042	Mid	10	55	0,953	0,387
Thin mangrove canopy	0,43 to 1	High	11	55	0,040	0,208
Dense mangrove canopy	0,43 to 1	High	12	55	1,212	0,920

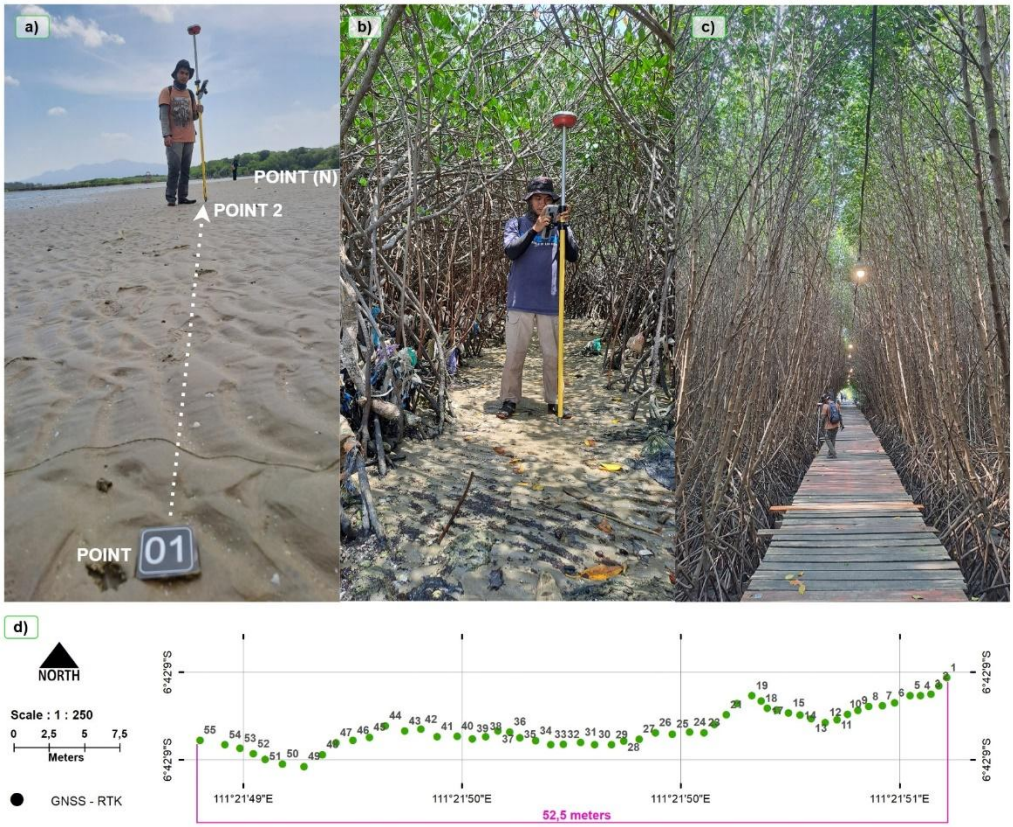

Fig. 2. (a) RTK data collecting was performed in an open sandy beach setting, encompassing points 1 to 55, (b) RTK point capture conducted in sparse canopy circumstances, demonstrating difficulties associated with partial vegetative cover, (c) Dense canopy conditions required the use of a bridge to get ground control points in obstructed locations, (d) Summary of a location where 55 RTK points were effectively obtained, illustrating diverse topography and vegetation cover conditions.

3.3. LIDAR-derived DTM accuracy assessment

The 3D Scanner application on an iPhone 12 Pro was utilized to gather LiDAR-based field data for this research. The application stored georeferenced information in an XYZ format. Ground Control Points (GCPs) in CloudCompare, an open-source LiDAR processing software, were utilized to calibrate the raw data and ensure excellent spatial accuracy. Upon meticulous rectification, the dataset was converted into a raster format, facilitating the extraction of precise pixel values essential for constructing a robust Digital Terrain Model (DTM). The subsequent phase involved integrating Real-Time Kinematic (RTK) survey points with the LiDAR-generated Digital Terrain Model (DTM) utilizing ArcGIS Pro. This facilitated a comprehensive comparison. The meticulously structured dataset in Excel provided the basis for extensive statistical studies. A comprehensive accuracy assessment and error analysis were conducted in Excel to ensure the reliability and precision of the elevation data obtained from the LiDAR device. This multi-step strategy enables the use of consumer-grade devices for high-accuracy topographic mapping in challenging field situations by integrating modern mobile sensor technology with meticulous data processing and validation techniques.

This study meticulously assessed the accuracy of the Digital Elevation Model (DEM) obtained by LiDAR by comparing GNSS survey data with LiDAR measurements collected via an iPhone across a 55-point cross-section comprising 12 distinct locations (**Fig. 3**). We employed significant statistical metrics to ascertain the accuracy of the outcomes.

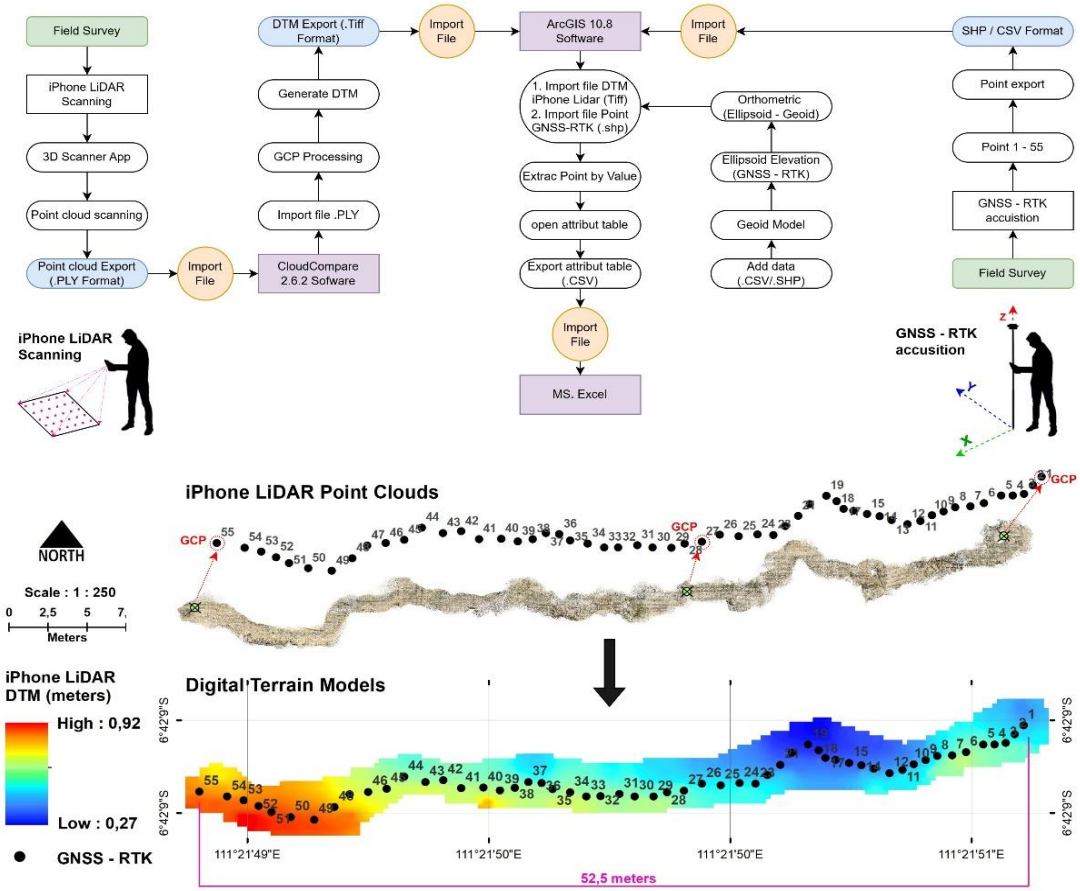

Fig. 3. The process includes building a DTM utilizing the iPhone 12 Pro LiDAR, corroborating it with GNSS-RTK data, and subsequently producing CSV data for Excel importation.

The metrics considered are Root Mean Square mistake (RMSE) (Gollob et al., 2021b), which assesses the magnitude of the overall mistake; Mean Absolute Error (MAE), which evaluates the average absolute deviation; and Bias (King et al., 2022, 2023; Kottner et al., 2023), which identifies systematic bias in elevation estimations. The Pearson Correlation Coefficient (r) was utilized to determine the strength and direction of the linear relationship between GNSS and LiDAR-derived elevations. Confidence Intervals (CI) of 95% were computed for each error metric to enhance the reliability evaluation (King et al., 2023b; B. Song et al., 2023). Confidence intervals are an effective method for quantifying uncertainty. This comprehensive validation methodology ensures the accuracy of the LiDAR-derived DEM, enabling its application in high-resolution topographic mapping. This enhances the use of mobile LiDAR technology in geospatial analysis. While a box plot does not explicitly present the standard deviation (B. Song et al., 2023; Vogt et al., 2021), it facilitates its estimation and offers valuable insights into the data distribution, variability, and potential outliers.

$$MAE = (1/n)\sum(i = 1)^{n}|y_i - \hat{y}_i| \quad (1)$$

where y_i denotes the observed value, $\hat{y}_i$ represents the predicted value, and n indicates the total number of observations.

$$Bias = (1/n)\sum(i = 1)^{n}(y_i - \hat{y}_i) \quad (2)$$

where y_i is the observed value, $\hat{y}_i$ is the predicted value, and n denotes the total number of observations.

$$RMSE = \sqrt{(1/n)\sum(i=1)^n(y_i - \hat{y}_i)^2} \quad (3)$$

where y_i represents observed values, $\hat{y}_i$ denotes predicted values, and n is the number of observations.

$$r = [\, n\sum(xy) - (\sum x)(\sum y)\,] / \sqrt{[n\sum x^2 - (\sum x)^2][n\sum y^2 - (\sum y)^2]} \quad (4)$$

where x *and* y are paired observed and predicted values, respectively, and n is the sample size.

4. RESULTS AND DISCUSSIONS

4.1. Positional Accuracy of iPhone 12 Pro Across Varying Vegetation Densities

The findings indicate that the positional accuracy of the iPhone 12 Pro, when adjusted with three Ground Control Points (GCPs) per location, is significantly affected by canopy cover environments. In unobstructed environments, the device operates at peak efficiency, providing a low mean absolute error (MAE < 0.1 m), a strong correlation with GNSS RTK data (up to r = 0.989), and negligible bias and RMSE−especially at Locations 3, 4, and 5−indicating accuracy to GNSS RTK in clear settings. Nonetheless, precision diminishes beneath medium-density canopy cover. Some places, such as Location 9, exhibit a robust correlation (r = 0.918) and a low mean absolute error (MAE) of 0.086 m, whereas others, like Location 10, demonstrate considerable deterioration, with an MAE of 0.381 m, a root mean square error (RMSE) of 0.482 m, and a weak correlation (r = 0.329). Performance is least effective in densely canopied regions, where errors significantly increase (e.g., Location 6: MAE = 1.064 m, bias = 0.928 m), and correlation may become negative (e.g., Location 12: r = -0.078), suggesting positional estimates are inconsistent with real movement or location. The findings indicate that the iPhone 12 Pro is inadequate for high-precision mapping in densely vegetated areas, while it demonstrates significant promise for accurate placement in open or semi-open regions (**Table 2**).

Table 2.
Summary statistics of GNSS RTK and iPhone 12 Pro location estimates at each site under different canopy conditions, including their mean values for the entire observation.

Canopy criteria	Site	MAE (meters)	Bias (meters)	Pearson Correlation Coefficient (r)	RMSE (m)	Bias (m)
No canopy covered	1	0,137	0,137	0,579	0,156	-0,137
	2	0,166	-0,164	0,693	0,190	0,164
	3	0,039	-0,035	0,782	0,045	0,035
	4	0,058	0,058	0,982	0,061	-0,058
	5	0,082	0,082	0,989	0,085	-0,082
medium-density canopy-covered	7	0,154	-0,028	0,514	0,168	0,028
	9	0,086	-0,011	0,918	0,107	0,012
	10	0,381	0,232	0,329	0,482	0,232
dense canopy covered	6	1,064	0,928	0,726	0,963	0,928
	8	0,121	0,077	0,092	0,276	-0,077
	11	0,234	-0,138	0,307	0,371	-0,138
	12	0,345	0,240	-0,078	0,489	-0,249

Elevation analysis of the Coastal Sand Beach and mangrove canopy zones indicates differing accuracy levels between the DTM_IP12 model and GNSS-RTK readings, significantly affected by topographic and surface features. In flat, unobstructed beach regions (e.g., Site 1 and Site 3), DTM_IP12 demonstrates great consistency and negligible variation from RTK data (median differences <0.05 m), signifying robust model reliability. Discrepancies arise in regions characterized by micro-topographic complexity or transitional surfaces (e.g., Site 2 and Site 5), where DTM_IP12 frequently overestimates or underestimates elevations by as much as ±0.2 m. In low-canopy mangrove areas, precision fluctuates with surface roughness and flora diversity. Sites 7 and 9 provide strong concordance, however Site 10 shows a significant overestimation (~±0.3 m), presumably attributable to residual canopy interference despite thin categorization. Under dense mangrove cover, performance markedly deteriorates, exhibiting increased vertical spreads and outliers in DTM outputs (e.g., Site 6 and Site 12), attributable to signal distortion caused by dense vegetation. Nonetheless, several locations (e.g., Site 8) have a strong correlation between methodologies, underscoring localized effectiveness in areas where vegetation and topography are generally homogeneous. The accuracy of DTM_IP12 is significantly dependent on vegetation density and surface complexity, with model performance diminishing in diverse or densely vegetated areas (**Fig. 4**).

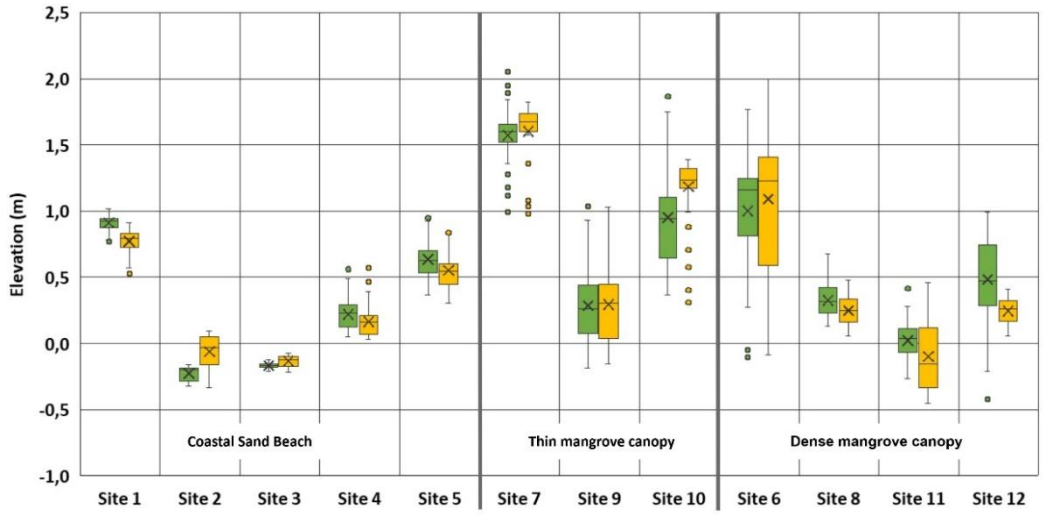

Fig. 4. Performance Comparison of Elevation RTK (green) and iPhone 12 (yellow) Models Across Coastal Sand Beach, thin mangrove canopy, and dense mangrove canopy in Microtopography.

4.2. Interplay Between Canopy Density and UAV-Derived Horizontal and Vertical Accuracy

In open field circumstances (**Fig. 5**, sites 1 to 5), the horizontal accuracy regularly exceeds that of dense mangrove areas, indicating enhanced positioning precision where canopy interference is limited. Nonetheless, the vertical precision in these broad fields poses issues, since minor topographic discrepancies occur more frequently than in thick mangrove areas. For example, Site 1 shows a little vertical variation of 0.5 meters between datasets utilizing Ground Control Network (GCN) and those lacking Ground Control Points (GCPs), while presenting a substantial horizontal disagreement of 11 meters. Conversely, Site 9, distinguished by minimal canopy cover, exhibits a vertical discrepancy of 3.1 meters and a horizontal error of 1.5 meters, signifying a significant influence of vegetation on positional precision. Site 11, characterized by a dense mangrove canopy, exhibits the greatest vertical variation of 4.2 meters, while displaying a comparatively minimal horizontal variance of 1 meter. These findings highlight the intricate relationship between canopy density and the location precision gained from UAVs. Although broad fields enhance horizontal accuracy, vertical precision is uneven due to variations in terrain.

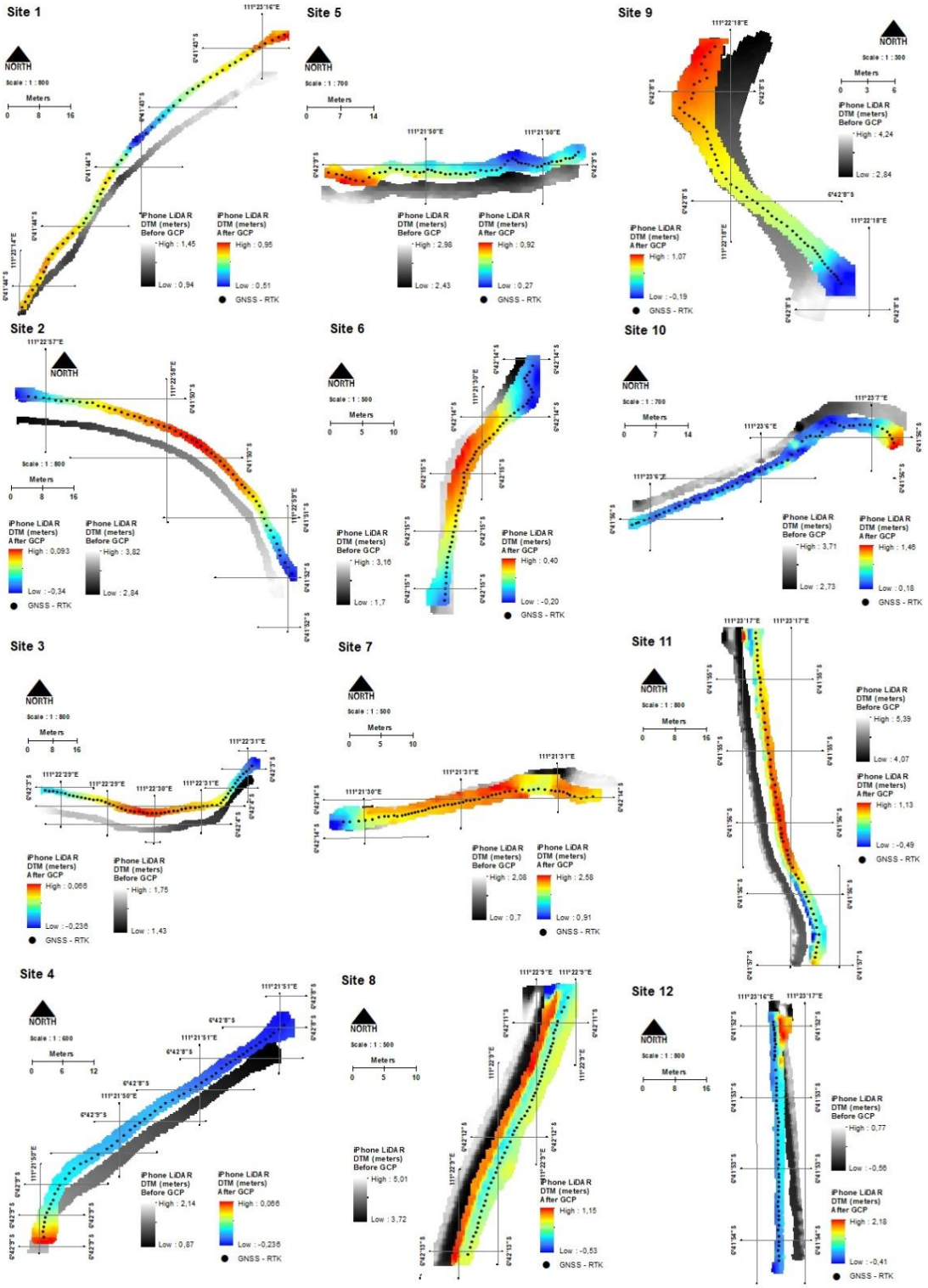

Fig. 5. The LiDAR-generated point cloud from the iPhone, including XYZ correction in CloudCompare (CC), produces a Digital Terrain Model (DTM) prior to Ground Control Point (GCP) correction (white to black) and subsequent to GCP correction (red to blue), with the DTM matching with RTK data.

In contrast, dense canopies present considerable vertical obstacles but may mitigate horizontal drift owing to their uniform construction. These results are essential for enhancing UAV data collection methodologies in diverse coastal settings. **Fig. 6** delineates the discrepancies in elevation measurements between the DTM iPhone GCP - No GCP and the RTK survey.

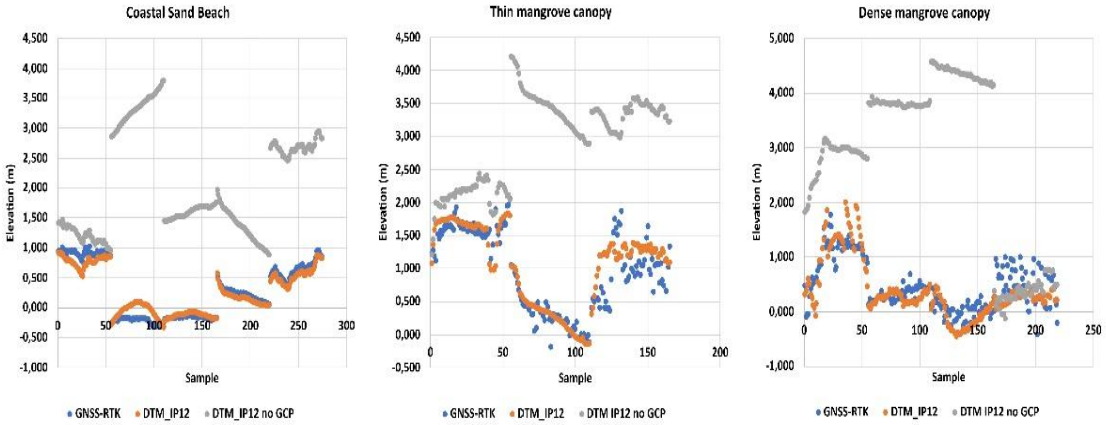

Fig. 6. The elevation value is assessed under three scenarios: open, sparse, and dense mangrove canopy; data conditions include RTK, DTM iPhone with GCP correction, and DTM iPhone without GCP.

4.3. Development and Application of Correction Models for iPhone LiDAR Elevation Data Across Varying Vegetation Densities

The elevation data acquired by iPhone LiDAR were juxtaposed with high-precision GNSS-RTK measurements to assess accuracy across three land cover categories: open fields, sparse mangrove canopies, and dense mangrove canopies. Linear regression analysis yielded correction formula tailored to each situation, demonstrating a substantial association in open areas ($R^2 = 0.956$), a moderate correlation in thin canopies ($R^2 = 0.7991$), and a weaker correlation in dense canopies ($R^2 = 0.663$). These correction models enable the proper calibration of iPhone LiDAR elevation data to achieve RTK-level precision (**Fig. 7**). This method improves the functionality of mobile LiDAR sensors, especially in coastal and mangrove regions where dense foliage might affect measurement accuracy. Utilizing these methods, researchers can conduct swift and reasonably precise elevation evaluations without requiring cumbersome or costly apparatus. Furthermore, including these models into data pipelines or mobile applications provides a pragmatic, scalable approach for conducting field surveys in intricate and dynamic settings, hence enhancing comprehensive environmental monitoring initiatives.

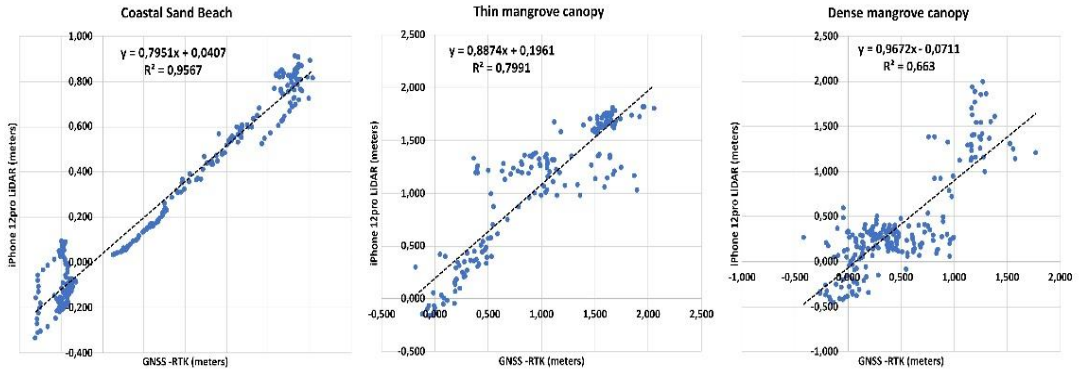

Fig. 7. Scatterplots showing elevation correction equations derived from iPhone LiDAR and GNSS-RTK data across open fields, thin mangrove canopy, and dense canopy conditions.

5. DISCUSSION

Creating a Digital Terrain Model (DTM) in mangrove ecosystems presents considerable difficulties for traditional techniques like GNSS, photogrammetry, and total stations, owing to the dense canopy and challenging topography (Basyuni, Amelia, et al., 2025; Basyuni et al., 2023; Basyuni, Mubaraq, et al., 2025; Wirasatriya et al., 2022). Although drone photogrammetry is effective for surface mapping, it frequently yields biased elevation data (Basyuni, Mubaraq, et al., 2025; Wirasatriya et al., 2022). LiDAR provides excellent precision; yet, it is expensive and presents dangers to equipment in saline conditions (Grottoli et al., 2021; Rogers et al., 2020; Zhang & Zhu, 2023). An option is iPhone-based LiDAR scanning, offering a cost-effective, efficient, and low-risk method that captures topography data (King et al., 2022, 2023b; Luetzenburg et al., 2021) over distances of 25 to 150 meters each scan. Its portability and compatibility with waterproof casings render it appropriate for mangrove environments, presenting significant potential for DTM creation. Scatter plot-derived linear regression equations ($Y = aX + b$) serve as an effective calibration function to adjust iPhone LiDAR elevation (Z) data in relation to GNSS-RTK standards.

The coefficient of determination (R^2) measures the strength of the association, revealing a high correlation in open areas ($R^2 = 0.956$), a moderate correlation in sparse mangrove canopies ($R^2 = 0.7991$), and a lesser correlation beneath dense canopies ($R^2 = 0.663$). The fluctuations indicate that vegetation density influences LiDAR accuracy. The regression equations provide a robust correction strategy, particularly in open and semi-obstructed situations, enhancing the applicability of smartphone-based LiDAR for forthcoming elevation research in various coastal contexts. This linear regression model can be advanced into an allometric model contingent upon land circumstances (NDVI, canopy density, automatic classification), facilitating economical and rapid topographic mapping utilizing mobile LiDAR. This methodology can function as a foundation for calibrating image-based machine learning and mobile elevation data.

In difficult site conditions characterized by steep slopes and deep forest, the full-waveform Riegl LMS-Q560 LiDAR, affixed to a DA42 MPP aircraft, achieved robust DTM accuracy (RMSE 0.15–0.62 m), Notwithstanding diminished point densities, effective interpolation techniques (NN, TPS) maintained model accuracy, confirming LiDAR's dependability for ecological and forestry purposes (Cățeanu & Ciubotaru, 2021). Although LiDAR and UAS photogrammetry exhibit similar vertical accuracy in unobstructed environments (±0.03 to ±0.06 m RMSE) (Rogers et al., 2020), this study's results indicate a systematic escalation in error beneath vegetative cover, with average RMSE values of 0.107 m in open regions, 0.252 m under medium-density canopies, and 0.525 m under dense canopies, highlighting the substantial influence of vegetation complexity on DSM accuracy.

In alignment with the results of (Luetzenburg et al., 2021), our research similarly indicates that the LiDAR sensor of the iPhone 12 Pro attains a remarkable RMSE of ±1 cm for small objects (side length > 10 cm) and ±10 cm for larger models (130 × 15 × 10 m), thereby reinforcing its viability as a cost-efficient substitute for conventional remote sensing methods in geoscientific applications. (King et al., 2023b) illustrate that the iPhone 12 Pro LiDAR (iLiDAR) mounted on a DJI Phantom 4 quadcopter offers a viable low-cost solution for snow depth estimation, attaining a root mean square error (RMSE) of 3 cm and an absolute mean error of 2.5 cm relative to conventional snow ruler measurements, underscoring its potential for accurate and economical snow monitoring. (King et al., 2022) further validated its high precision (RMSE ~6 mm), indicating its applicability for citizen research initiatives.

The findings of this investigation corroborate and enhance existing knowledge regarding the reliability of consumer-grade Apple LiDAR systems, while also demonstrating their applicability in creating Digital Terrain Models (DTMs) of mangroves with varying canopy densities. Previous studies have consistently shown that iPhone and iPad LiDAR achieve centimetric to sub-centimetric accuracy in both controlled and open settings, with inaccuracies increasing during dynamic data collection and extensive spatial coverage due to cumulative pose and SLAM-related drift (Luetzenburg et al., 2021; Teo & Yang, 2023). Significant accuracy has been recorded in various

applications, such as snow depth estimation, forensic documentation, anthropometry, and rapid environmental monitoring, with biases and RMSE values typically remaining under 1 cm (King et al., 2022; Kottner et al., 2023; Mikalai et al., 2022). The method by which applications handle data is the paramount aspect influencing the ultimate quality of the metrics. Applications such as PIX4DCatch and SiteScape, which exhibit robust drift control and global orientation, consistently outperform their counterparts. Conversely, the 3D Scanner App and EveryPoint are more prone to errors due to noise and orientation during extended scans (Corradetti et al., 2022; Teppati Losè et al., 2022).

The present results align with these tendencies, indicating enhanced DTM accuracy in open mangrove areas, intermediate precision under sparse canopies, and considerable decline in dense vegetation due to occlusion, signal attenuation, and vertical bias. These constraints illustrate the challenges of employing mobile LiDAR in wetlands with intricate structures, although they also indicate potential improvements through enhanced acquisition techniques and allometric correction. While professional LiDAR remains superior in dense canopies, the iPhone 12 Pro LiDAR presents a robust, cost-effective alternative for high-resolution Digital Terrain Model mapping in mangrove regions characterized by sparse to moderate vegetation. It additionally facilitates scalable and accessible MRV applications.

6. CONCLUSIONS

This research demonstrates that iPhone LiDAR can generate dependable and accurate Digital Terrain Models (DTMs), especially when supplemented by GNSS-RTK Ground Control Points (GCPs). In dense canopy conditions, GNSS signals often deteriorate, leading to possible inaccuracies and vertical bias. Nonetheless, iPhone LiDAR ensures data consistency across diverse contexts, particularly in aquatic and exceptionally dark circumstances. The robust correlation (R^2) seen in open field circumstances indicates that these locations can be relied upon to rectify iPhone LiDAR-generated DTMs. Moreover, employing allometric equations presents a viable alternative for rectifying terrain data in the absence of GNSS-based ground control points, offering a cost-effective method to enhance survey accuracy without compromising data integrity. This method possesses considerable promise for extensive environmental mapping and monitoring applications, particularly in financially limited or logistically difficult regions.

ACKNOWLEDGEMENT

This research is supported by Faculty of Fisheries and Marine Science, Diponegoro University with contract number: 20/UN7.F10/PP/VII/2025.

REFERENCES

Alongi, D. M. (2022). Impacts of Climate Change on Blue Carbon Stocks and Fluxes in Mangrove Forests. Forests, 13(2), 149. https://doi.org/10.3390/f13020149

Amelia, R., Basyuni, M., Alfinsyahri, A., Sulistiyono, N., Slamet, B., Bimantara, Y., Harahap, S. S. H., Harahap, M., Harahap, I. M., Al Mustaniroh, S. S., Sasmito, S. D., & Arifanti, V. B. (2023). Evaluation of Plant Growth and Potential of Carbon Storage in the Restored Mangrove of an Abandoned Pond in Lubuk Kertang, North Sumatra, Indonesia. Forests, 14(1). https://doi.org/10.3390/f14010158

Amuyou, U. A., Wang, Y., Ebuta, B. F., Iheaturu, C. J., & Antonarakis, A. S. (2022). Quantification of Above-Ground Biomass over the Cross-River State, Nigeria, Using Sentinel-2 Data. Remote Sensing, 14(22). https://doi.org/10.3390/rs14225741

Arifanti, V. B., Kauffman, J. B., Subarno, J. B., Ilman, M., Tosiani, A., & Novita, N. (2022). Contributions of mangrove conservation and restoration to climate change mitigation in Indonesia. Global Change Biology, 28(15), 4523‑4538. https://doi.org/10.1111/gcb.16216

Arnaud, M., Krause, S., Norby, R. J., Dang, T. H., Acil, N., Kettridge, N., Gauci, V., & Ullah, S. (2023). Global mangrove root production, its controls and roles in the blue carbon budget of mangroves. In Global Change Biology (Vol. 29, Issue 12, pp. 3256‑3270). John Wiley and Sons Inc. https://doi.org/10.1111/gcb.16701

Bagas, A., Trinida, P., Muskananfola, M. R., Febrianto, S., & Ayuningrum, D. (2024). Analysis of shoreline change along the coast of Rembang, Indonesia, using digital shoreline analysis system. In Songklanakarin J. Sci. Technol (Vol. 46, Issue 5).

Basyuni, M., Amelia, R., Aznawi, A. A., Wirasatriya, A., Iryanthony, S. B., Slamet, B., Al Mustaniroh, S. S., Rahmania, R., Rahmila, Y. I., Sumarga, E., Larekeng, S. H., Salmo, S., Kajita, T., Sivaipram, I., & Ali, H. M. (2025). Reduction of mangrove carbon stock ecosystems due to illegal logging using a combination of unmanned aerial vehicle imagery and field surveys. Global Journal of Environmental Science and Management, 11(1), 225‑242. https://doi.org/10.22034/gjesm.2025.01.14

Basyuni, M., Mubaraq, A., Amelia, R., Wirasatriya, A., Iryanthony, S. B., Slamet, B., Al Mustaniroh, S. S., Pradisty, N. A., Sidik, F., Hanintyo, R., Sumarga, E., Larekeng, S. H., Salmo, S. G., Kajita, T., Ali, H. M., Sakti, A. D., & Arifanti, V. B. (2025). Mangrove aboveground biomass estimation using UAV imagery and a constructed height model in Budeng‑Perancak, Bali, Indonesia. Ecological Informatics, 86. https://doi.org/10.1016/j.ecoinf.2025.103037

Basyuni, M., Wirasatriya, A., Iryanthony, S. B., Amelia, R., Slamet, B., Sulistiyono, N., Pribadi, R., Sumarga, E., Eddy, S., Al Mustaniroh, S. S., Sasmito, S. D., Sidik, F., Kajita, T., Ali, H. M., Macklin, P. A., & Arifanti, V. B. (2023). Aboveground biomass and carbon stock estimation using UAV photogrammetry in Indonesian mangroves and other competing land uses. Ecological Informatics, 77. https://doi.org/10.1016/j.ecoinf.2023.102227

Bernstein, T., & Janssen, V. (2022). Determining Positional Uncertainty of NRTK Observations for Inclusion in the GDA2020 State Adjustment. In New South Wales.

Bimrah, K., Dasgupta, R., Hashimoto, S., Saizen, I., & Dhyani, S. (2022). Ecosystem Services of Mangroves: A Systematic Review and Synthesis of Contemporary Scientific Literature. In Sustainability (Switzerland) (Vol. 14, Issue 19). MDPI. https://doi.org/10.3390/su141912051

Cățeanu, M., & Ciubotaru, A. (2021). The effect of lidar sampling density on dtm accuracy for areas with heavy forest cover. Forests, 12(3), 1‑20. https://doi.org/10.3390/f12030265

Chan, E. P. Y., Fung, T., & Wong, F. K. K. (2021). Estimating above-ground biomass of subtropical forest using airborne LiDAR in Hong Kong. Scientific Reports, 11(1). https://doi.org/10.1038/s41598-021-81267-8

Corradetti, A., Seers, T., Mercuri, M., Calligaris, C., Busetti, A., & Zini, L. (2022). Benchmarking Different SfM-MVS Photogrammetric and iOS LiDAR Acquisition Methods for the Digital Preservation of a Short-Lived Excavation: A Case Study from an Area of Sinkhole Related Subsidence. Remote Sensing, 14(20). https://doi.org/10.3390/rs14205187

Di Stefano, F., Chiappini, S., Gorreja, A., Balestra, M., & Pierdicca, R. (2021). Mobile 3D scan LiDAR: a literature review. In Geomatics, Natural Hazards and Risk (Vol. 12, Issue 1, pp. 2387‑2429). Taylor and Francis Ltd. https://doi.org/10.1080/19475705.2021.1964617

Donato, D.C.; Kauffman, J.B.; Murdiyarso, D.; Kurnianto, S.; Stidham, M.; Kanninen, M. (2011) Mangroves among the most carbon-rich forests in the tropics. Nature Geoscience, 4 (5), 293‑297. http://dx.doi.org/10.1038/ngeo1123

Donato, D.C.; Kauffman, J.B.; Mackenzie, R.A.; Ainsworth, A.; Pfleeger, A.Z. (2012) Whole-island carbon stocks in the tropical Pacific: Implications for mangrove conservation and upland restoration. Journal of Environmental Management, 97 (1), 89‑96. http://dx.doi.org/10.1016/j.jenvman.2011.12.004

Feng, T., Chen, S., Feng, Z., Shen, C., & Tian, Y. (2021). Effects of canopy and multi-epoch observations on single-point positioning errors of a GNSS in coniferous and broadleaved forests. Remote Sensing, 13(12). https://doi.org/10.3390/rs13122325

Friess Daniel A, Kerrylee Rogers, Catherine E. Lovelock, Ken W. Krauss, Stuart E. Hamilton, Shing Yip Lee, Richard Lucas, Jurgenne Primavera, Anusha Rajkaran, & Suhua Shi. (2019). Daniel A. Friess_2019_compressed. Annual Reviews, 44, 89‑115. https://doi.org/https://doi.org/10.1146/annurev-environ-101718-033302

Gao, L., Chai, G., & Zhang, X. (2022). Above-Ground Biomass Estimation of Plantation with Different Tree Species Using Airborne LiDAR and Hyperspectral Data. Remote Sensing, 14(11). https://doi.org/10.3390/rs14112568

Giri, C., Ochieng, E., Tieszen, L. L., Zhu, Z., Singh, A., Loveland, T., Masek, J., & Duke, N. (2011). Status and distribution of mangrove forests of the world using earth observation satellite data. Global Ecology and Biogeography, 20(1), 154‐159. https://doi.org/10.1111/j.1466-8238.2010.00584.x

Gollob, C., Ritter, T., Kraßnitzer, R., Tockner, A., & Nothdurft, A. (2021a). Measurement of forest inventory parameters with apple ipad pro and integrated lidar technology. Remote Sensing, 13(16). https://doi.org/10.3390/rs13163129

Gollob, C., Ritter, T., Kraßnitzer, R., Tockner, A., & Nothdurft, A. (2021b). Measurement of forest inventory parameters with apple ipad pro and integrated lidar technology. Remote Sensing, 13(16). https://doi.org/10.3390/rs13163129

Grottoli, E., Biausque, M., Rogers, D., Jackson, D. W. T., & Cooper, J. A. G. (2021). Structure-from-motion-derived digital surface models from historical aerial photographs: A new 3d application for coastal dune monitoring. Remote Sensing, 13(1), 1‐22. https://doi.org/10.3390/rs13010095

Hu, T., Zhang, Y. Y., Su, Y., Zheng, Y., Lin, G., & Guo, Q. (2020). Mapping the global mangrove forest aboveground biomass using multisource remote sensing data. Remote Sensing, 12(10). https://doi.org/10.3390/rs12101690

Iryanthony, S. B., Wirasatriya, A., Pribadi, R., Purnomo, P. W., Muchtar, E., Basyuni, M., & Wijayanto, D. (2025). High-resolution Unmanned Aerial Vehicles (UAV) imagery for estimating above and below-ground biomass in mangroves of Rembang, Central Java, Indonesia. Biodiversitas, 26(5), 2065‐2078. https://doi.org/10.13057/biodiv/d260505

Iryanthony, S. B., Wirasatriya, A., Pribadi, R., Wahyu Purnomo, P., Mukhtar, E., Basyuni, M., & Wijayanto, D. (2025). High-Resolution UAV-Based Mapping and Species Identification of Mangroves in Pasar Banggi, Rembang, Central Java. IOP Conference Series: Earth and Environmental Science, 1496(1). https://doi.org/10.1088/1755-1315/1496/1/012012

Ji, S., Liu, G., Weng, D., Wang, Z., He, K., & Chen, W. (2022). Single-Epoch Ambiguity Resolution of a Large-Scale CORS Network with Multi-Frequency and Multi-Constellation GNSS. Remote Sensing, 14(15). https://doi.org/10.3390/rs14153819

Jurado, J. M., Ramos, M. I., Enríquez, C., & Feito, F. R. (2020). The impact of canopy reflectance on the 3D structure of individual trees in a Mediterranean Forest. Remote Sensing, 12(9). https://doi.org/10.3390/RS12091430

Kauffman, J.B.; Bernardino, A.B.; Ferreira, T.O.; Giovannoni, L.R.; Gomes, L.E.O.; Romero, D.J.; Jimenez, L.C.Z.; Ruiz, F. (2018) Carbon stocks of mangroves and salt marshes of the Amazon region, Brazil. Biology Lettters, 20180208. http://dx.doi.org/10.1098/rsbl.2018.0208

Kanellopoulos, N., Pantazis, G., & Lambrou, E. (2019). Distance Limitations when using CORS Networks and GNSS Receivers for Deformation Monitoring.

King, F., Kelly, R., & Fletcher, C. G. (2022). Evaluation of LiDAR-Derived Snow Depth Estimates From the iPhone 12 Pro. IEEE Geoscience and Remote Sensing Letters, 19. https://doi.org/10.1109/LGRS.2022.3166665

King, F., Kelly, R., & Fletcher, C. G. (2023a). New opportunities for low-cost LiDAR-derived snow depth estimates from a consumer drone-mounted smartphone. Cold Regions Science and Technology, 207. https://doi.org/10.1016/j.coldregions.2022.103757

King, F., Kelly, R., & Fletcher, C. G. (2023b). New opportunities for low-cost LiDAR-derived snow depth estimates from a consumer drone-mounted smartphone. Cold Regions Science and Technology, 207. https://doi.org/10.1016/j.coldregions.2022.103757

Kottner, S., Thali, M. J., & Gascho, D. (2023). Using the iPhone’s LiDAR technology to capture 3D forensic data at crime and crash scenes. Forensic Imaging, 32. https://doi.org/10.1016/j.fri.2023.200535

Krause, S., Sanders, T. G. M., Mund, J. P., & Greve, K. (2019). UAV-based photogrammetric tree height measurement for intensive forest monitoring. Remote Sensing, 11(7). https://doi.org/10.3390/rs11070758

Li, Z., Lu, T., Yu, K., & Wang, J. (2023). Interpolation of GNSS Position Time Series Using GBDT, XGBoost, and RF Machine Learning Algorithms and Models Error Analysis. Remote Sensing, 15(18). https://doi.org/10.3390/rs15184374

Lovelock, C. E., Barbier, E., & Duarte, C. M. (2022). Tackling the mangrove restoration challenge. PLoS Biology, 20(10). https://doi.org/10.1371/journal.pbio.3001836

Luetzenburg, G., Kroon, A., & Bjørk, A. A. (2021). Evaluation of the Apple iPhone 12 Pro LiDAR for an Application in Geosciences. Scientific Reports, 11(1). https://doi.org/10.1038/s41598-021-01763-9

Lynch, J. C., Winn, N., Kovalenko, K., & Guntenspergen, G. (2024). Comparing Wetland Elevation Change Using a Surface Elevation Table, Digital Level, and Total Station. Estuaries and Coasts, 47(7), 2071‐2079. https://doi.org/10.1007/s12237-023-01263-1

Mcleod, E.; Chmura, G.L.; Bouillon, S.; Salm, R.; Björk, M.; Duarte, C.M.; Lovelock, C.E.; Schlesinger, W.H.; Silliman, B.R. (2011) A blueprint for blue carbon: Toward an improved understanding of the role of vegetated coastal habitats in sequestering CO2. Frontiers in Ecology and the Environment, 9, 552-560. https://doi.org/10.1890/110004

Mêda, P., Calvetti, D., & Sousa, H. (2023). Exploring the Potential of iPad-LiDAR Technology for Building Renovation Diagnosis: A Case Study. Buildings, 13(2). https://doi.org/10.3390/buildings13020456

Mikalai, Z., Andrey, D., Hawas, H. S., Tetiana, H., & Oleksandr, S. (2022). Human body measurement with the iPhone 12 Pro LiDAR scanner. AIP Conference Proceedings, 2430. https://doi.org/10.1063/5.0078310

Murtiyoso, A., Grussenmeyer, P., Landes, T., & Macher, H. (2021). First assessments into the use of commercial-grade solid state lidar for low cost heritage documentation. International Archives of the Photogrammetry, Remote Sensing and Spatial Information Sciences - ISPRS Archives, 43(B2-2021), 599‑604. https://doi.org/10.5194/isprs-archives-XLIII-B2-2021-599-2021

Mustofa, V. M., Soenardjo, N., & Pratikto, I. (2023). Analisis Tekstur Sedimen terhadap Kelimpahan Gastropoda di Ekosistem Mangrove Desa Pasar Banggi, Rembang. Journal of Marine Research, 12(1), 137‑143. https://doi.org/10.14710/jmr.v12i1.35003

Nik Azhan Hakim, N. N. A., Razali, R., Mohd Said, M. S., Muhamad, M. A. H., Abdul Rahim, H., & Mokhtar, M. A. (2023). Accuracy Assessment on Detail Survey Plan Using iPhone 13 Pro Max LiDAR Sensor. International Journal of Geoinformatics, 19(5), 79‑86. https://doi.org/10.52939/ijg.v19i5.2665

Paul, S., Siddiqua, F., & Tayung, K. (2023). Exploration of Mangroves Associated Microbes for Bioactive Metabolites. INTERNATIONAL JOURNAL OF PLANT AND ENVIRONMENT, 9(03), 202‑209. https://doi.org/10.18811/ijpen.v9i03.03

Pepe, M. (2018). Cors architecture and evaluation of positioning by low-cost gnss receiver. Geodesy and Cartography, 44(2), 36‑44. https://doi.org/10.3846/gac.2018.1255

Raza, by M., Hassan, A., Khan, M., Emad, M., Saki, S., & Raza, M. (2023). A critical comparison of interpolation techniques for digital terrain modelling in mining Correspondence to: Dates: How to cite: ORCID. The Journal of the Southern African Institute of Mining and Metallurgy, 123(2), 53‑62. https://doi.org/10.17159/2411

Razali, M. I., Idris, A. N., Razali, M. H., & Syafuan, W. M. (2022). Quality Assessment of 3D Point Clouds on the Different Surface Materials Generated from iPhone LiDAR Sensor. International Journal of Geoinformatics, 18(4), 51‑58. https://doi.org/10.52939/ijg.v18i4.2259

Rogers, S. R., Manning, I., & Livingstone, W. (2020). Comparing the spatial accuracy of digital surface models from four unoccupied aerial systems: Photogrammetry versus lidar. Remote Sensing, 12(17), 1‑17. https://doi.org/10.3390/rs12172806

Sasmito, S. D., Basyuni, M., Kridalaksana, A., Saragi-Sasmito, M. F., Lovelock, C. E., & Murdiyarso, D. (2023). Challenges and opportunities for achieving Sustainable Development Goals through restoration of Indonesia ' s mangroves. Nature Ecology and Evolution, 7(1), 62‑70. https://doi.org/10.1038/s41559-022-01926-5

Shapiro, A. (2024). Mangroves. In Cloud-Based Remote Sensing with Google Earth Engine (pp. 1023‑1043). Springer International Publishing. https://doi.org/10.1007/978-3-031-26588-4_47

Soeprobowati, T. R., Sularto, R. B., Hadiyanto, H., Puryono, S., Rahim, A., Jumari, J., & Gell, P. (2024). The carbon stock potential of the restored mangrove ecosystem of Pasarbanggi, Rembang, Central Java. Marine Environmental Research, 193. https://doi.org/10.1016/j.marenvres.2023.106257

Song, B., Kim, J., Kwon, H., Kim, S., Oh, S. H., Ha, Y., & Song, S. H. (2023). Smartphone-Based LiDAR Application for Easy and Accurate Wound Size Measurement. Journal of Clinical Medicine, 12(18). https://doi.org/10.3390/jcm12186042

Song, S., Ding, Y., Li, W., Meng, Y., Zhou, J., Gou, R., Zhang, C., Ye, S., Saintilan, N., Krauss, K. W., Crooks, S., Lv, S., & Lin, G. (2023). Mangrove reforestation provides greater blue carbon benefit than afforestation for mitigating global climate change. Nature Communications, 14(1). https://doi.org/10.1038/s41467-023-36477-1

Suwa, R., Rollon, R., Sharma, S., Yoshikai, M., Albano, G. M. G., Ono, K., Adi, N. S., Ati, R. N. A., Kusumaningtyas, M. A., Kepel, T. L., Maliao, R. J., Primavera-Tirol, Y. H., Blanco, A. C., & Nadaoka, K. (2021). Mangrove biomass estimation using canopy height and wood density in the South East and East Asian regions. Estuarine, Coastal and Shelf Science, 248. https://doi.org/10.1016/j.ecss.2020.106937

Teo, T. A., & Yang, C. C. (2023). Evaluating the accuracy and quality of an iPad Pro ' s built-in lidar for 3D indoor mapping. Developments in the Built Environment, 14. https://doi.org/10.1016/j.dibe.2023.100169

Teppati Losè, L., Spreafico, A., Chiabrando, F., & Giulio Tonolo, F. (2022). Apple LiDAR Sensor for 3D Surveying: Tests and Results in the Cultural Heritage Domain. Remote Sensing, 14(17). https://doi.org/10.3390/rs14174157

Tian, Y., Huang, H., Zhou, G., Zhang, Q., Xie, X., Ou, J., Zhang, Y., Tao, J., & Lin, J. (2023). Mangrove Biodiversity Assessment Using UAV Lidar and Hyperspectral Data in China's Pinglu Canal Estuary. In Remote Sensing (Vol. 15, Issue 10). https://doi.org/10.3390/rs15102622

Tomaštík, J., & Everett, T. (2023). Static Positioning under Tree Canopy Using Low-Cost GNSS Receivers and Adapted RTKLIB Software. Sensors, 23(6). https://doi.org/10.3390/s23063136

Tong, P., Yang, X., Yang, Y., Liu, W., & Wu, P. (2023). Multi-UAV Collaborative Absolute Vision Positioning and Navigation: A Survey and Discussion. Drones, 7(4). https://doi.org/10.3390/drones7040261

Vogt, M., Rips, A., & Emmelmann, C. (2021a). Comparison of iPad Pro®'s LiDAR and TrueDepth Capabilities with an Industrial 3D Scanning Solution. Technologies, 9(2). https://doi.org/10.3390/technologies9020025

Vogt, M., Rips, A., & Emmelmann, C. (2021b). Comparison of iPad Pro®'s LiDAR and TrueDepth Capabilities with an Industrial 3D Scanning Solution. Technologies, 9(2). https://doi.org/10.3390/technologies9020025

Wainwright, B. J., Millar, T., Bowen, L., Semon, L., Hickman, K. J. E., Lee, J. N., Yeo, Z. Y., & Zahn, G. (2023). The core mangrove microbiome reveals shared taxa potentially involved in nutrient cycling and promoting host survival. Environmental Microbiome, 18(1), 1–12. https://doi.org/10.1186/s40793-023-00499-5

Wirasatriya, A., Pribadi, R., Iryanthony, S. B., Maslukah, L., Sugianto, D. N., Helmi, M., Ananta, R. R., Adi, N. S., Kepel, T. L., Ati, R. N. A., Kusumaningtyas, M. A., Suwa, R., Ray, R., Nakamura, T., & Nadaoka, K. (2022). Mangrove Above-Ground Biomass and Carbon Stock in the Karimunjawa-Kemujan Islands Estimated from Unmanned Aerial Vehicle-Imagery. Sustainability (Switzerland), 14(2). https://doi.org/10.3390/su14020706

Yang, W., Liu, Y., & Liu, F. (2020). An improved relative gnss tracking method utilizing single frequency receivers. Sensors (Switzerland), 20(15), 1–19. https://doi.org/10.3390/s20154073

Yurdakul, Ö., & Kalaycı, İ. (2022). The effect of GLONASS on position accuracy in CORS-TR measurements at different baseline distances. International Journal of Engineering and Geosciences, 7(3), 229–246. https://doi.org/10.26833/ijeg.975204

Zeybek, M., Taşkaya, S., Elkhrachy, I., & Tarolli, P. (2023). Improving the Spatial Accuracy of UAV Platforms Using Direct Georeferencing Methods: An Application for Steep Slopes. Remote Sensing, 15(10). https://doi.org/10.3390/rs15102700

Zhang, Z., & Zhu, L. (2023). A Review on Unmanned Aerial Vehicle Remote Sensing: Platforms, Sensors, Data Processing Methods, and Applications. In Drones (Vol. 7, Issue 6). MDPI. https://doi.org/10.3390/drones7060398

Zvirgzds, J., & Celms, A. (2020). GNSS RTK Performance Improvements using Galileo Satellite Signal. Latvian Journal of Physics and Technical Sciences, 57(1–2), 78–84. https://doi.org/10.2478/lpts-2020-0010